

Variational Bayesian Approach and Gauss-Markov-Potts prior model

Camille Chapdelaine^{1,2}

¹ Laboratoire des signaux et systèmes, CNRS, CentraleSupélec-Université Paris Saclay, Gif-sur-Yvette, France

² SAFRAN SA, Safran Tech, Pôle Technologie du Signal et de l'Information, Magny-Les-Hameaux, France

June 2018

1 Introduction

In many inverse problems such as 3D X-ray Computed Tomography (CT) [1], the estimation of an unknown quantity, such as a volume or an image, can be greatly enhanced, compared to maximum-likelihood techniques [2, 3, 4, 5, 6], by incorporating a prior model on the quantity to reconstruct.

This prior model is often defined in terms of sparsity on the unknown in some domain, for instance sparsity of one of its derivative [7, 8], of a wavelet transform [9, 10], or of its representation in a learnt dictionary [11, 12]. A more complex prior can be designed for multi-channel estimation such as reconstruction and segmentation thanks to Gauss-Markov-Potts prior model [13, 14, 15, 16, 17].

For very large inverse problems such as 3D X-ray CT, maximization a posteriori (MAP) techniques are often used due to the huge size of the data and the unknown [18, 19, 20]. Nevertheless, MAP estimation does not enable to have quantify uncertainties on the retrieved reconstruction, which can be useful for post-reconstruction processes for instance in industry and medicine. In X-ray CT, a method has been proposed in [21] to estimate exact uncertainties but can only be applied to few pixels of interest. More recently, in [22], an estimation of confidence regions for MAP estimator is detailed, but is difficult to apply for joint reconstruction and segmentation algorithms [17]. Another way to tackle the problem of uncertainties estimation is to compute posterior mean (PM) for which the uncertainties are the variances of the posterior distribution. Because MCMC methods are not affordable for very large 3D problems, this paper presents an algorithm to jointly estimate the reconstruction and the uncertainties by computing PM thanks to variational Bayesian approach (VBA) [23, 24]. The prior model we consider for the unknowns is a Gauss-Markov-Potts prior which has been shown to give good results in many inverse problems [13, 25, 26, 16, 17, 27]. After having detailed the used prior models, the algorithm based on VBA is detailed : it corresponds to an iterative computation of approximate distributions through the iterative updates of their parameters. The updating formulae are given in the last section. We also provide a method for initialization of the algorithm, as a method to fix each parameter. Perspectives are applications of this algorithm to large 3D problems such as 3D X-ray CT.

2 Prior models

2.1 Forward model

We consider a general forward model for linear inverse problems, accounting for uncertainties

$$\mathbf{g} = \mathbf{H}\mathbf{f} + \boldsymbol{\zeta} \quad (1)$$

For instance, this forward model is used in 3D X-ray CT : \mathbf{f} is the volume to reconstruct, and is discretized in $N = N_x \times N_y \times N_z$ voxels. We denote by M = the number of measurements, which is the size of \mathbf{g} . In 3D X-ray CT, matrix \mathbf{H} , which is size $M \times N$, is called the projection operator or projector. Its adjoint \mathbf{H}^T is called the backprojection operator or backprojector. Uncertainties $\boldsymbol{\zeta}$ are modeled as Gaussian [28]

$$p(\zeta_i | \rho_{\zeta_i}) = \mathcal{N}(\zeta_i | 0, \rho_{\zeta_i}^{-1}) \quad (2)$$

A conjugate prior is assigned to inverse variances ρ_{ζ} :

$$p(\rho_{\zeta_i} | \alpha_{\zeta_0}, \beta_{\zeta_0}) = \mathcal{G}(\rho_{\zeta_i} | \alpha_{\zeta_0}, \beta_{\zeta_0}). \quad (3)$$

\mathcal{G} denotes Gamma distribution

$$\mathcal{G}(\rho_{\zeta_i} | \alpha_{\zeta_0}, \beta_{\zeta_0}) = \frac{\beta_{\zeta_0}^{\alpha_{\zeta_0}}}{\Gamma(\alpha_{\zeta_0})} \rho_{\zeta_i}^{\alpha_{\zeta_0}-1} \exp[-\beta_{\zeta_0} \rho_{\zeta_i}], \rho_{\zeta_i} > 0, \forall i \quad (4)$$

where Γ is Euler's gamma function.

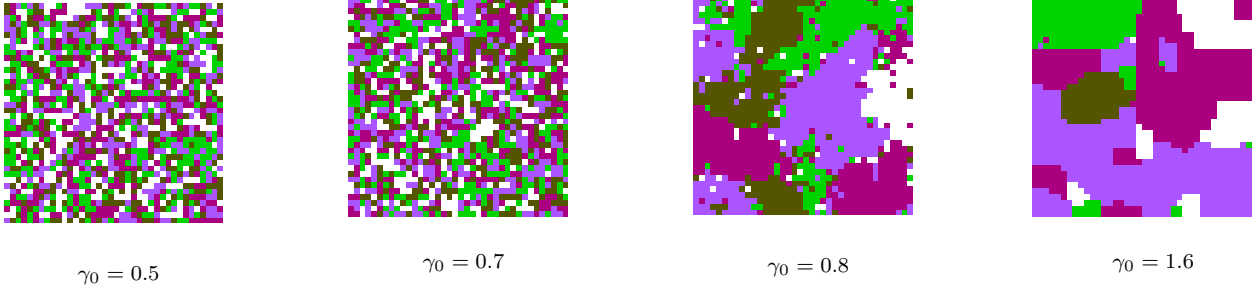


Figure 1: Potts fields \mathbf{z} for different values of γ_0

2.2 Gauss-Markov-Potts prior model for the volume

Gauss-Markov-Potts prior model introduces a dependance of f_j on the material in which voxel j is [14, 29, 27]. Each voxel is assigned a label z_j which is $z_j = k$ if voxel j is in material k , $k \in \mathbb{N}$, $1 \leq k \leq K$. K is the number of materials and is supposed to be known. Given the material of voxel j , we have the following prior for f_j :

$$f_j \sim \mathcal{N}(m_k, \rho_k^{-1}) \text{ if } z_j = k. \quad (5)$$

Means and inverse variances of the classes are unknown and are assigned a conjugate prior :

$$p(m_k | m_0, v_0) = \mathcal{N}(m_k | m_0, v_0) \quad (6)$$

and

$$p(\rho_k | \alpha_0, \beta_0) = \mathcal{G}(\rho_k | \alpha_0, \beta_0) \quad (7)$$

where m_0 , v_0 , α_0 et β_0 are fixed parameters.

A Potts prior is assigned to labels \mathbf{z} in order to promote compact regions in the volume [13, 15, 17, 27]. Using Hammersley-Clifford theorem [30], this prior reads [15, 16, 17] :

$$p(\mathbf{z} | \boldsymbol{\alpha}, \gamma_0) \propto \exp \left[\sum_{j=1}^N \left(\sum_{k=1}^K \alpha_k \delta(z_j - k) + \gamma_0 \sum_{i \in \mathcal{V}(j)} \delta(z_j - z_i) \right) \right] \quad (8)$$

where [15]

$$\sum_{k=1}^K \exp[\alpha_k] = 1. \quad (9)$$

Parameter γ_0 is called Potts coefficient or granularity coefficient [31, 32, 33, 34, 17]. It tunes the compacity of the classes, as shown in figure 1. Partition function for \mathbf{z} is

$$Z(\boldsymbol{\alpha}, \gamma_0) = \sum_{\mathbf{z}' \in \{1, \dots, K\}^N} \exp \left[\sum_{j=1}^N \left(\sum_{k=1}^K \alpha_k \delta(z'_j - k) + \gamma_0 \sum_{i \in \mathcal{V}(j)} \delta(z'_j - z'_i) \right) \right] \quad (10)$$

and is untractable [35, 34].

3 Bayesian inference and variational Bayesian approach

Based on prior models \mathcal{M} described in section 2, the joint posterior distribution of the unknowns

$$\boldsymbol{\psi} = (\mathbf{f}, \boldsymbol{\rho}_\zeta, \mathbf{z}, \mathbf{m}, \boldsymbol{\rho}) \quad (11)$$

reads, according to Bayes' rule

$$\begin{aligned} p(\boldsymbol{\psi} | \mathbf{g}; \mathcal{M}) &= p(\mathbf{f}, \boldsymbol{\rho}_\zeta, \mathbf{z}, \mathbf{m}, \boldsymbol{\rho} | \mathbf{g}; \mathcal{M}) \\ &= \frac{p(\mathbf{g}; \boldsymbol{\psi} | \mathcal{M})}{p(\mathbf{g} | \mathcal{M})} = \frac{p(\mathbf{g}; \mathbf{f}, \boldsymbol{\rho}_\zeta, \mathbf{z}, \mathbf{m}, \boldsymbol{\rho} | \mathcal{M})}{p(\mathbf{g} | \mathcal{M})} \\ &= \frac{p(\mathbf{g} | \mathbf{f}, \boldsymbol{\rho}_\zeta) p(\mathbf{f} | \mathbf{z}, \mathbf{m}, \boldsymbol{\rho}) p(\boldsymbol{\rho}_\zeta | \alpha_{\zeta_0}, \beta_{\zeta_0}) p(\mathbf{z} | \boldsymbol{\alpha}, \gamma_0) p(\mathbf{m} | m_0, v_0) p(\boldsymbol{\rho} | \alpha_0, \beta_0)}{p(\mathbf{g} | \mathcal{M})} \end{aligned} \quad (12)$$

where

$$p(\mathbf{g} | \mathbf{f}, \boldsymbol{\rho}_\zeta) = (2\pi)^{-\frac{M}{2}} \det(\mathbf{V}_\zeta)^{-1/2} \exp \left[-\frac{1}{2} \|\mathbf{g} - \mathbf{H}\mathbf{f}\|_{\mathbf{V}_\zeta}^2 \right], \quad (13)$$

$$p(\mathbf{f}|\mathbf{z}, \mathbf{m}, \boldsymbol{\rho}) = (2\pi)^{-\frac{N}{2}} \det(\mathbf{V}\mathbf{z})^{-1/2} \exp\left[-\frac{1}{2}\|\mathbf{f} - \mathbf{m}\mathbf{z}\|_{\mathbf{V}\mathbf{z}}^2\right], \quad (14)$$

$$p(\boldsymbol{\rho}_\zeta|\alpha_{\zeta_0}, \beta_{\zeta_0}) = \frac{\beta_{\zeta_0}^{\alpha_{\zeta_0}}}{\Gamma(\alpha_{\zeta_0})} \exp\left[\sum_{i=1}^M ((\alpha_{\zeta_0} - 1) \ln \rho_{\zeta_i} - \beta_{\zeta_0} \rho_{\zeta_i})\right], \quad (15)$$

$$p(\mathbf{z}|\boldsymbol{\alpha}, \gamma_0) = \frac{1}{Z(\boldsymbol{\alpha}, \gamma_0)} \exp\left[\sum_j \left(\sum_{k=1}^K \alpha_k \delta(z_j - k) + \gamma_0 \sum_{i \in \mathcal{V}(j)} \delta(z_j - z_i)\right)\right] \quad (16)$$

$$p(\mathbf{m}|m_0, v_0) = (2\pi)^{-\frac{K}{2}} v_0^{-\frac{K}{2}} \exp\left[-\frac{1}{2v_0} \sum_{k=1}^K (m_k - m_0)^2\right], \quad (17)$$

$$p(\boldsymbol{\rho}|\alpha_0, \beta_0) = \frac{\beta_0^{\alpha_0}}{\Gamma(\alpha_0)} \exp\left[\sum_{k=1}^K ((\alpha_0 - 1) \ln \rho_k - \beta_0 \rho_k)\right]. \quad (18)$$

where $v_{\zeta_i} = \rho_{\zeta_i}^{-1}$, $m_{z_j} = m_k$ and $v_{z_j} = \rho_k^{-1}$ if $z_j = k$, $\mathbf{V}\mathbf{z} = \text{diag}[\mathbf{v}\mathbf{z}]$, and $\mathbf{V}_\zeta = \text{diag}[\mathbf{v}_\zeta]$. The evidence $p(\mathbf{g}|\mathcal{M})$ does not depend on the unknowns.

In [17], an algorithm is proposed to compute the Maximum-A-Posteriori (MAP) estimator for this posterior distribution in 3D X-ray CT. Another possible estimator in decision theory is Minimum Mean-Square Error (MMSE), which is Posterior Mean (PM). The calculation of PM can be achieved by MCMC methods which generate samples of the posterior distribution (12), typically using a Gibbs sampler [26, 16]. The problem is that the computational complexity of these methods is unaffordable in large 3D inverse problems such as 3D X-ray CT [16, 17]. Variational Bayesian approach (VBA) enables to alleviate the cost for PM calculation, by computing an analytical approximation of the true posterior distribution (12) [23, 24]. This approximation is chosen sufficiently simple to compute PM. For instance, it can be a fully-factorized density, which corresponds to mean-field approximation (MFA) [24]. VBA is known to well-estimate PM by computing an approximate posterior distribution [36, 24, 22]. Once its factorization is chosen, the approximate posterior distribution q has to minimize Kullback-Leibler divergence [23, 24] :

$$KL(q(\boldsymbol{\psi})||p(\boldsymbol{\psi}|\mathbf{g})) = \int_{\boldsymbol{\psi}} q(\boldsymbol{\psi}) \ln\left(\frac{q(\boldsymbol{\psi})}{p(\boldsymbol{\psi}|\mathbf{g})}\right) d\boldsymbol{\psi} = \ln(p(\mathbf{g}|\mathcal{M})) - \mathcal{F}(q(\boldsymbol{\psi})) \quad (19)$$

where

$$\begin{aligned} \mathcal{F}(q(\boldsymbol{\psi})) &= \int_{\boldsymbol{\psi}} q(\boldsymbol{\psi}) \ln\left(\frac{p(\mathbf{g}, \boldsymbol{\psi})}{q(\boldsymbol{\psi})}\right) d\boldsymbol{\psi} \\ &= - \int_{\boldsymbol{\psi}} q(\boldsymbol{\psi}) \ln(q(\boldsymbol{\psi})) d\boldsymbol{\psi} + \int_{\boldsymbol{\psi}} q(\boldsymbol{\psi}) \ln(p(\mathbf{g}, \boldsymbol{\psi})) d\boldsymbol{\psi} \end{aligned} \quad (20)$$

is free negative energy [23, 15]. The entropy of approximate posterior distribution q is defined as

$$\mathcal{H}(q(\boldsymbol{\psi})) = - \int_{\boldsymbol{\psi}} q(\boldsymbol{\psi}) \ln(q(\boldsymbol{\psi})) d\boldsymbol{\psi}. \quad (21)$$

In the next section, we present an algorithm implementing VBA for computing PM with Gauss-Markov-Potts prior model.

4 Variational Bayesian Approach with Gauss-Markov-Potts prior

For

$$\boldsymbol{\psi} = (\mathbf{f}, \boldsymbol{\rho}_\zeta, \mathbf{z}, \mathbf{m}, \boldsymbol{\rho}),$$

we choose an approximate posterior distribution of the form

$$\begin{aligned} q(\mathbf{f}, \boldsymbol{\rho}_\zeta, \mathbf{z}, \mathbf{m}, \boldsymbol{\rho}) &= \prod_{j=1}^N q_{f_j}(f_j|z_j) \times \prod_{j=1}^N q_{z_j}(z_j) \\ &\times \prod_{i=1}^M q_{\rho_{\zeta_i}}(\rho_{\zeta_i}) \times \prod_{k=1}^K q_{m_k}(m_k) \times \prod_{k=1}^K q_{\rho_k}(\rho_k). \end{aligned} \quad (22)$$

This approximation performs a partial separation, since the dependence between f_j and z_j is preserved [15]. In our experiments, we have noticed an unsteady behaviour if this dependence is broken. This is because separating f_j and z_j leads to a too gross approximation [24].

Minimizing Kullback-Leibler divergence with respect to each factor leads to

$$\left\{ \begin{array}{l} q_{f_j}(f_j|z_j = k) = \mathcal{N}(f_j|\tilde{m}_{jk}, \tilde{v}_{jk}), \forall k \\ q_{z_j}(z_j) = \frac{\exp[\sum_{k=1}^K (\tilde{\alpha}_{jk} + \gamma_0 \sum_{i \in \mathcal{V}(j)} q_{z_i}(k)) \delta(z_j - k)]}{\sum_{k=1}^K \exp[\tilde{\alpha}_{jk} + \gamma_0 \sum_{i \in \mathcal{V}(j)} q_{z_i}(k)]} \\ q_{\rho_{\zeta_i}}(\rho_{\zeta_i}) = \mathcal{G}(\rho_{\zeta_i}|\tilde{\alpha}_{\zeta_{0_i}}, \tilde{\beta}_{\zeta_{0_i}}) \\ q_{m_k}(m_k) = \mathcal{N}(m_k|\tilde{m}_{0_k}, \tilde{v}_{0_k}) \\ q_{\rho_k}(\rho_k) = \mathcal{G}(\rho_k|\tilde{\alpha}_{0_k}, \tilde{\beta}_{0_k}) \end{array} \right. \quad (23)$$

where $q_{z_i}(k)$ in the expression of $q_{z_j}(k)$ is the value of $q_{z_i}(k)$ at previous iteration. The algorithm in figure 2 turns into an iterative updating of the parameters of the distributions in equation (23). The updating formulae are given hereafter.

We introduce *digamma* function

$$\psi(x) = \frac{\Gamma'(x)}{\Gamma(x)}, \quad (24)$$

as the expectation of number N_k of voxels in class k with respect to approximate distribution q

$$\mathbb{E}_{q_{\mathbf{Z}}}(N_k(\mathbf{Z})) = \sum_{j=1}^N q_{z_j}(k), \quad (25)$$

and several auxiliary variables :

$$\left\{ \begin{array}{l} \tilde{m}_j = \sum_{k=1}^K \tilde{m}_{jk} q_{z_j}(k) \\ \tilde{v}_j = \sum_{k=1}^K \tilde{v}_{jk} q_{z_j}(k) \\ \tilde{m}_j^{(2)} = \sum_{k=1}^K (\tilde{m}_{jk} - \tilde{m}_j)^2 q_{z_j}(k) = \sum_{k=1}^K \tilde{m}_{jk}^2 q_{z_j}(k) - \tilde{m}_j^2 \\ \tilde{v}_j^{(2)} = \tilde{v}_j + \tilde{m}_j^{(2)} \\ \tilde{v}_{\zeta_i} = \frac{\tilde{\beta}_{\zeta_{0_i}}}{\tilde{\alpha}_{\zeta_{0_i}}} \end{array} \right. \quad (26)$$

and $\tilde{\mathbf{V}}_{\zeta} = \text{diag}[\tilde{v}_{\zeta}]$.

After calculations, the entropy of approximate distribution q reads

$$\begin{aligned} \mathcal{H}(q(\mathbf{f}, \boldsymbol{\rho}_{\zeta}, \mathbf{z}, \mathbf{m}, \boldsymbol{\rho})) &= \frac{N}{2}(1 + \ln(2\pi)) + \frac{1}{2} \sum_{j=1}^N \sum_{k=1}^K \ln(\tilde{v}_{jk}) q_{z_j}(k) - \sum_{j=1}^N \sum_{k=1}^K q_{z_j}(k) \ln(q_{z_j}(k)) \\ &+ \sum_{i=1}^M \left[\ln(\Gamma(\tilde{\alpha}_{\zeta_{0_i}})) - \ln(\tilde{\beta}_{\zeta_{0_i}}) + \tilde{\alpha}_{\zeta_{0_i}} - (\tilde{\alpha}_{\zeta_{0_i}} - 1) \psi(\tilde{\alpha}_{\zeta_{0_i}}) \right] \\ &+ \frac{K}{2}(1 + \ln(2\pi)) + \frac{1}{2} \sum_{k=1}^K \ln(\tilde{v}_{0_k}) + \sum_{k=1}^K \left[\ln(\Gamma(\tilde{\alpha}_{0_k})) - \ln(\tilde{\beta}_{0_k}) + \tilde{\alpha}_{0_k} - (\tilde{\alpha}_{0_k} - 1) \psi(\tilde{\alpha}_{0_k}) \right] \end{aligned} \quad (27)$$

and the expectation of the joint distribution of the data and the unknowns, with respect to approximate distribution q , is

$$\begin{aligned} \mathbb{E}_q(\ln(p(\mathbf{g}; \mathbf{f}, \boldsymbol{\rho}_{\zeta}, \mathbf{z}, \mathbf{m}, \boldsymbol{\rho}|\mathcal{M}))) &= -\frac{M}{2} \ln(2\pi) - \frac{1}{2} \sum_{i=1}^M \left[\ln(\tilde{\beta}_{\zeta_{0_i}}) - \psi(\tilde{\alpha}_{\zeta_{0_i}}) \right] \\ &- \frac{1}{2} \|\mathbf{g} - \mathbf{H}\tilde{\mathbf{m}}\|_{\tilde{\mathbf{V}}_{\zeta}}^2 - \frac{1}{2} \sum_{j=1}^N \tilde{v}_j^{(2)} \left[\mathbf{H}^T \tilde{\mathbf{V}}_{\zeta}^{-1} \mathbf{H} \right]_{jj} \\ &- \frac{N}{2} \ln(2\pi) - \frac{1}{2} \sum_{j=1}^N \sum_{k=1}^K \left(\frac{\tilde{\alpha}_{0_k}}{\tilde{\beta}_{0_k}} \left[\tilde{v}_{jk} + \tilde{v}_{0_k} + (\tilde{m}_{jk} - \tilde{m}_{0_k})^2 \right] + \ln(\tilde{\beta}_{0_k}) - \psi(\tilde{\alpha}_{0_k}) \right) q_{z_j}(k) \\ &- \ln(Z(\boldsymbol{\alpha}, \gamma_0)) + \sum_{j=1}^N \sum_{k=1}^K \left(\alpha_k + \gamma_0 \sum_{i \in \mathcal{V}(j)} q_{z_i}(k) \right) q_{z_j}(k) \\ &- M (\ln(\Gamma(\alpha_{\zeta_0})) - \alpha_{\zeta_0} \ln(\beta_{\zeta_0})) - (\alpha_{\zeta_0} - 1) \sum_{i=1}^M (\ln(\tilde{\beta}_{\zeta_{0_i}}) - \psi(\tilde{\alpha}_{\zeta_{0_i}})) - \beta_{\zeta_0} \sum_{i=1}^M \frac{\tilde{\alpha}_{\zeta_{0_i}}}{\tilde{\beta}_{\zeta_{0_i}}} \end{aligned}$$

$$\begin{aligned}
& -\frac{K}{2} \ln(2\pi v_0) - \frac{1}{2v_0} \sum_{k=1}^K \left(\tilde{v}_{0_k} + (\tilde{m}_{0_k} - m_0)^2 \right) \\
& - K (\ln(\Gamma(\alpha_0)) - \alpha_0 \ln(\beta_0)) - (\alpha_0 - 1) \sum_{k=1}^K (\ln(\tilde{\beta}_{0_k}) - \psi(\tilde{\alpha}_{0_k})) - \beta_0 \sum_{k=1}^K \frac{\tilde{\alpha}_{0_k}}{\tilde{\beta}_{0_k}}.
\end{aligned} \tag{28}$$

The stopping criterion of the algorithm in figure 2 is free negative energy :

$$\mathcal{F}(q(\mathbf{f}, \rho_\zeta, \mathbf{z}, \mathbf{m}, \rho)) = \mathcal{H}(q(\mathbf{f}, \rho_\zeta, \mathbf{z}, \mathbf{m}, \rho)) + \mathbb{E}_q(\ln(p(\mathbf{g}; \mathbf{f}, \rho_\zeta, \mathbf{z}, \mathbf{m}, \rho | \mathcal{M}))) \tag{29}$$

from which constants are removed. At the end of the algorithm, the unknowns are estimated by their expectation according to the approximate distribution, excepted for the labels which are estimated by maximum a posteriori, due to the fact that they are discrete variables :

$$\begin{cases} \hat{z}_j = \arg \max_k \{q_{z_j}(k)\} \\ \hat{f}_j = \tilde{m}_{j_k} \text{ avec } k = \hat{z}_j \\ \hat{\rho}_{\zeta_i} = \frac{\tilde{\alpha}_{\zeta_{0_i}}}{\tilde{\beta}_{\zeta_{0_i}}} \\ \hat{m}_k = \tilde{m}_{0_k} \\ \hat{\rho}_k = \frac{\tilde{\alpha}_{0_k}}{\tilde{\beta}_{0_k}} \end{cases} \tag{30}$$

In the algorithm, the updating order of the parameters of approximate distributions is important. This order is shown in figure 2. The distributions of the variables which are approximated as independent are immediatly replaced by their updates. On the opposite, the updating of joint approximate distribution of the volume and the labels

$$q_{\mathbf{f}, \mathbf{z}}^{(t)}(\mathbf{f}, \mathbf{z}) = q_{\mathbf{f}}^{(t)}(\mathbf{f} | \mathbf{z}) q_{\mathbf{z}}^{(t)}(\mathbf{z}) \tag{31}$$

involves two steps : the update of $q_{\mathbf{f}}$ and the one of $q_{\mathbf{z}}$. For this reason, $q_{\mathbf{z}}^{(t)}(\mathbf{z})$ is updated using $q_{\mathbf{f}}^{(t-1)}(\mathbf{f} | \mathbf{z})$.

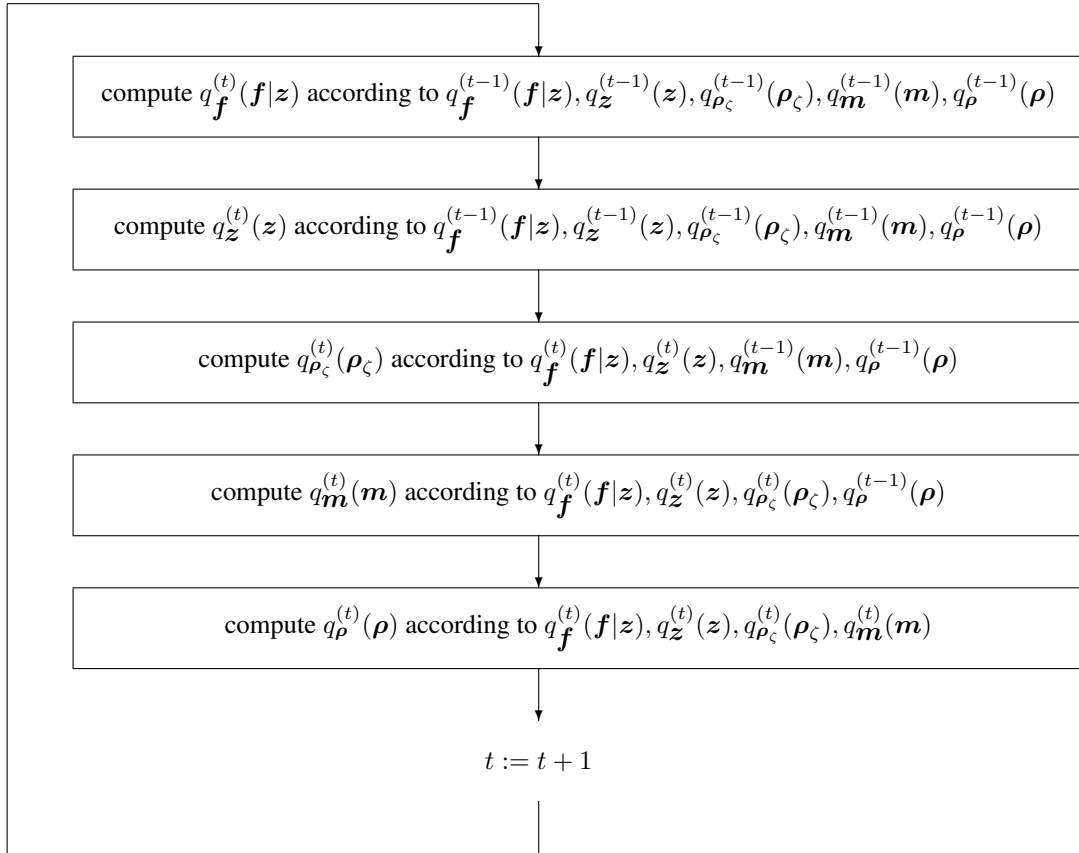


Figure 2: Iterative algorithm to compute approximating distribution $q(\mathbf{f}, \rho_\zeta, \mathbf{z}, \mathbf{m}, \rho)$

4.1 Approximate distribution for the volume

By minimizing Kullback-Leibler divergence with respect to q_{f_j} , we have :

$$q_{f_j}(f_j|z_j = k) = \mathcal{N}(f_j|\tilde{m}_{jk}, \tilde{v}_{jk}), \forall j, \forall k \quad (32)$$

where

$$\begin{cases} \tilde{v}_{jk} = \left(\frac{\tilde{\alpha}_{0k}}{\tilde{\beta}_{0k}} + \left[\mathbf{H}^T \tilde{\mathbf{V}}_{\zeta}^{-1} \mathbf{H} \right]_{jj} \right)^{-1} \\ \tilde{m}_{jk} = \tilde{m}_j + \tilde{v}_{jk} \left(\frac{\tilde{\alpha}_{0k}}{\tilde{\beta}_{0k}} (\tilde{m}_{0k} - \tilde{m}_j) + \left[\mathbf{H}^T \tilde{\mathbf{V}}_{\zeta}^{-1} (\mathbf{g} - \mathbf{H}\tilde{\mathbf{m}}) \right]_j \right) \end{cases} \quad (33)$$

4.2 Approximate distribution for the labels

By minimizing Kullback-Leibler divergence with respect to q_{z_j} , we have :

$$q_{z_j}(z_j) = \frac{\exp \left[\sum_{k=1}^K \left(\tilde{\alpha}_{jk} + \gamma_0 \sum_{i \in \mathcal{V}(j)} q_{z_i}(k) \right) \delta(z_j - k) \right]}{\sum_{k=1}^K \exp \left[\tilde{\alpha}_{jk} + \gamma_0 \sum_{i \in \mathcal{V}(j)} q_{z_i}(k) \right]} \quad (34)$$

where $q_{z_i}(k), \forall i \in \mathcal{V}(j)$, is the value of $q_{z_i}(k)$ at the previous iteration of the algorithm presented in figure 2. We have

$$\begin{aligned} \tilde{\alpha}_{jk} = & \alpha_k - \frac{1}{2} \left(\frac{\tilde{\alpha}_{0k}}{\tilde{\beta}_{0k}} \left[\tilde{v}_{jk} + \tilde{v}_{0k} + (\tilde{m}_{jk} - \tilde{m}_{0k})^2 \right] + \ln(\tilde{\beta}_{0k}) - \psi(\tilde{\alpha}_{0k}) \right) \\ & - \frac{1}{2} \left((\tilde{v}_{jk} + \tilde{m}_{jk}^2) \left[\mathbf{H}^T \tilde{\mathbf{V}}_{\zeta}^{-1} \mathbf{H} \right]_{jj} - 2\tilde{m}_{jk} \left(\tilde{m}_j \left[\mathbf{H}^T \tilde{\mathbf{V}}_{\zeta}^{-1} \mathbf{H} \right]_{jj} + \left[\mathbf{H}^T \tilde{\mathbf{V}}_{\zeta}^{-1} (\mathbf{g} - \mathbf{H}\tilde{\mathbf{m}}) \right]_j \right) \right) \\ & + \frac{1}{2} \ln(\tilde{v}_{jk}) \end{aligned} \quad (35)$$

It is worth to notice that this step does not imply the calculation of diagonal coefficients $\left[\mathbf{H}^T \tilde{\mathbf{V}}_{\zeta}^{-1} \mathbf{H} \right]_{jj}, \forall j$, and of the back-projection of the errors, since they have been computed before to update the approximate distribution of the volume (see the algorithm shown in figure 2).

4.3 Approximate distribution of inverse variances of the uncertainties

By minimizing Kullback-Leibler divergence with respect to $q_{\rho_{\zeta_i}}$, we have :

$$q_{\rho_{\zeta_i}}(\rho_{\zeta_i}) = \mathcal{G}(\rho_{\zeta_i} | \tilde{\alpha}_{\zeta_{0i}}, \tilde{\beta}_{\zeta_{0i}}) \quad (36)$$

where parameters are updated by formulae :

$$\begin{cases} \tilde{\alpha}_{\zeta_{0i}} = \alpha_{\zeta_0} + \frac{1}{2} \\ \tilde{\beta}_{\zeta_{0i}} = \beta_{\zeta_0} + \frac{1}{2} \left((g_i - [\mathbf{H}\tilde{\mathbf{m}}]_i)^2 + \left(\mathbf{H}\tilde{\mathbf{V}}^{(2)} \mathbf{H}^T \right)_{ii} \right) \end{cases}, \forall i \in \{1, \dots, M\}. \quad (37)$$

and where $\tilde{\mathbf{V}}^{(2)} = \text{diag} \left[\tilde{v}^{(2)} \right]$.

4.4 Approximate distribution for the means of the classes

By minimizing Kullback-Leibler divergence with respect to q_{m_k} , we have :

$$q_{m_k}(m_k) = \mathcal{N}(m_k | \tilde{m}_{0k}, \tilde{v}_{0k}) \quad (38)$$

where

$$\begin{cases} \tilde{v}_{0k} = \left(\frac{1}{v_0} + \frac{\tilde{\alpha}_{0k}}{\tilde{\beta}_{0k}} \sum_{j=1}^N q_{z_j}(k) \right)^{-1} \\ \tilde{m}_{0k} = \tilde{v}_{0k} \left(\frac{m_0}{v_0} + \frac{\tilde{\alpha}_{0k}}{\tilde{\beta}_{0k}} \sum_{j=1}^N \tilde{m}_{jk} q_{z_j}(k) \right) \end{cases} \quad (39)$$

4.5 Approximate distribution for the inverses of variances of the classes

By minimizing Kullback-Leibler divergence with respect to q_{ρ_k} , we have :

$$q_{\rho_k}(\rho_k) = \mathcal{G}(\rho_k | \tilde{\alpha}_{0k}, \tilde{\beta}_{0k}) \quad (40)$$

where

$$\begin{cases} \tilde{\alpha}_{0k} = \alpha_0 + \frac{1}{2} \sum_{j=1}^N q_{z_j}(k) = \alpha_0 + \frac{1}{2} \mathbb{E}_{q_{\mathbf{Z}}} (N_k(\mathbf{Z})) \\ \tilde{\beta}_{0k} = \beta_0 + \frac{1}{2} \sum_{j=1}^N \left(\tilde{v}_{0k} + \tilde{v}_{jk} + (\tilde{m}_{jk} - \tilde{m}_{0k})^2 \right) q_{z_j}(k) \end{cases} \quad (41)$$

4.6 Fixing the parameters for Variational Bayesian Approach

The strategies to fix the parameters for VBA are different from JMAP, since a different estimator is computed. This is particularly the case for parameters $(\alpha_{\zeta_0}, \beta_{\zeta_0}, \alpha_0, \beta_0)$.

Through our experiments, Jeffreys' priors [37], which is non-informative, for ρ_ζ and ρ gives the best results [15]. Gamma distribution $\mathcal{G}(\rho|\alpha, \beta)$ is non-informative fixing $\alpha = 0$ et $\beta = 0$ but leads to improper prior. In order to keep our priors proper, $(\alpha_{\zeta_0}, \beta_{\zeta_0}, \alpha_0, \beta_0)$ are fixed near zero : $\alpha_{\zeta_0} \ll 1, \beta_{\zeta_0} \ll 1, \alpha_0 \ll 1$ and $\beta_0 \ll 1$. To take the SNR : *Signal-to-Noise Ratio* into account, we comply with the following relation

$$\mathbb{E}(\rho_{\zeta_i}|\alpha_{\zeta_0}, \beta_{\zeta_0}) = \frac{\alpha_{\zeta_0}}{\beta_{\zeta_0}} = \mathbb{E}(\rho_k|\alpha_0, \beta_0) \times 10^{\frac{SNR}{10}} = \frac{\alpha_0}{\beta_0} \times 10^{\frac{SNR}{10}}. \quad (42)$$

Moreover, in order to avoid "NaN"-values in our computations, $(\alpha_{\zeta_0}, \beta_{\zeta_0}, \alpha_0, \beta_0)$ are fixed such that

$$\frac{\alpha_{\zeta_0}}{\beta_{\zeta_0}} \leq 1 \text{ et } \frac{\alpha_0}{\beta_0} \leq 1. \quad (43)$$

Other parameters are fixed as in JMAP [17]. From initial volume $\mathbf{f}^{(0)}$, m_0 is fixed by

$$m_0 = \frac{1}{2} \left(\min_j f_j^{(0)} + \max_j f_j^{(0)} \right), \quad (44)$$

v_0 is fixed sufficiently large such that $m_k, \forall k$, can take all possible values in the set of gray levels of the volume, γ_0 is sufficiently large to promote compact classes, and, from initial segmentation $\mathbf{z}^{(0)}$ of $\mathbf{f}^{(0)}$, we fix

$$\alpha_k = \ln \left(\frac{N_k^{(0)}}{N} \right) \quad (45)$$

where $N_k^{(0)}$ is the number of voxels in class k in initial segmentation $\mathbf{z}^{(0)}$. Like in [17], the number of classes K is supposed to be known a priori.

4.7 Initialization

The initialization of the algorithm is crucial to ensure its convergence. Based on an initial reconstruction $\mathbf{f}^{(0)}$ obtained for instance by filtered backprojection [2], an initial segmentation $\mathbf{z}^{(0)}$ is performed by applying a fast method [38, 39, 40]. From this initial segmentation, initial means $\mathbf{m}^{(0)}$ and variances $\mathbf{v}^{(0)}$ of the classes are computed. We initialize means $\tilde{m}_{jk}, \forall j, k$ by $f_j^{(0)}$ if voxel j is in class k at initialization, and $m_k^{(0)}$ otherwise :

$$\tilde{m}_{jk}^{(0)} = \begin{cases} f_j^{(0)} & \text{if } z_j^{(0)} = k \\ m_k^{(0)} & \text{otherwise} \end{cases} \quad (46)$$

Probabilities to be in each class are initialized by 0 or 1 :

$$q_{z_j}(k)^{(0)} = \begin{cases} 1 & \text{if } z_j^{(0)} = k \\ 0 & \text{otherwise} \end{cases} \quad (47)$$

Inspired by their updating formula (33), we initialize variances \tilde{v}_{jk} by :

$$\tilde{v}_{jk}^{(0)} = \left(\frac{1}{v_k^{(0)}} + \frac{\alpha_{\zeta_0}}{\beta_{\zeta_0}} [\mathbf{H}^T \mathbf{H}]_{jj} \right)^{-1} \quad (48)$$

The approximate distributions of ρ_ζ , \mathbf{m} and ρ are initialized by their conditional distribution given the other unknowns. These expressions are given in [17] :

$$\tilde{\alpha}_{\zeta_{0i}}^{(0)} = \alpha_{\zeta_0} + \frac{1}{2}, \forall i, \quad (49)$$

$$\tilde{\beta}_{\zeta_{0i}}^{(0)} = \beta_{\zeta_0} + \frac{1}{2} \left(g_i - [\mathbf{H} \mathbf{f}^{(0)}]_i \right)^2, \forall i, \quad (50)$$

$$\tilde{v}_{0k}^{(0)} = \left(\frac{1}{v_0} + \frac{N_k^{(0)}}{v_k^{(0)}} \right)^{-1}, \forall k, \quad (51)$$

$$\tilde{m}_{0k}^{(0)} = \tilde{v}_{0k}^{(0)} \left(\frac{m_0}{v_0} + N_k^{(0)} \frac{m_k^{(0)}}{v_k^{(0)}} \right), \forall k, \quad (52)$$

$$\tilde{\alpha}_{0k}^{(0)} = \alpha_0 + \frac{N_k^{(0)}}{2}, \forall k, \quad (53)$$

$$\tilde{\beta}_{0k}^{(0)} = \beta_0 + \frac{N_k^{(0)}}{2} v_k^{(0)}, \forall k. \quad (54)$$

5 Conclusion and perspectives

In this paper, we have presented a full algorithm for joint estimation of reconstruction and uncertainties in linear inverse problems regularized by Gauss-Markov-Potts prior model. Perspectives for this work are applications to large 3D inverse problems such as 3D X-ray CT, for which implementation problems will be discussed in future works.

References

- [1] J. A. Fessler, “Statistical image reconstruction methods for transmission tomography,” *Handbook of medical imaging*, vol. 2, pp. 1–70, 2000.
- [2] L. Feldkamp, L. Davis, and J. Kress, “Practical cone-beam algorithm,” *JOSA A*, vol. 1, no. 6, pp. 612–619, 1984.
- [3] J. I. Jackson, C. H. Meyer, D. G. Nishimura, and A. Macovski, “Selection of a convolution function for Fourier inversion using gridding [computerized tomography application],” *Medical Imaging, IEEE Transactions on*, vol. 10, no. 3, pp. 473–478, 1991.
- [4] R. Gordon, R. Bender, and G. T. Herman, “Algebraic reconstruction techniques (ART) for three-dimensional electron microscopy and X-ray photography,” *Journal of theoretical Biology*, vol. 29, no. 3, pp. 471–481, 1970.
- [5] P. Gilbert, “Iterative methods for the three-dimensional reconstruction of an object from projections,” *Journal of theoretical biology*, vol. 36, no. 1, pp. 105–117, 1972.
- [6] A. H. Andersen and A. C. Kak, “Simultaneous algebraic reconstruction technique (SART): a superior implementation of the ART algorithm,” *Ultrasonic imaging*, vol. 6, no. 1, pp. 81–94, 1984.
- [7] E. Y. Sidky, H. Jakob, X. Pan, *et al.*, “Convex optimization problem prototyping for image reconstruction in computed tomography with the Chambolle & Pock algorithm,” *Physics in medicine and biology*, vol. 57, no. 10, p. 3065, 2012.
- [8] M. Storath, A. Weinmann, J. Friel, and M. Unser, “Joint image reconstruction and segmentation using the Potts model,” *Inverse Problems*, vol. 31, no. 2, p. 025003, 2015.
- [9] L. Wang, A. Mohammad-Djafari, and N. Gac, “X-ray computed tomography using a sparsity enforcing prior model based on haar transformation in a bayesian framework,” *Fundamenta Informaticae*, vol. 155, no. 4, pp. 449–480, 2017.
- [10] T. Notargiacomo, D. Houzet, G. Bernard, and V. Fristot, “Sparse Regularization of CBCT Reconstruction Using 3D Dual-Tree Complex Wavelet Transform and Dictionary Learning Techniques,” in *The 4th International Conference on Image Formation in X-Ray Computed Tomography*, 2016.
- [11] I. Y. Chun, Z. Xuehang, Y. Long, and J. A. Fessler, “Sparse View X-Ray CT Reconstruction Using l_1 Regularization with Learned Sparsifying Transforms,” in *The 14th International Meeting on Fully Three-Dimensional Image Reconstruction in Radiology and Nuclear Medicine*, 2017.
- [12] X. Zheng, S. Ravishankar, Y. Long, and J. A. Fessler, “Union of Learned Sparsifying Transforms Based Low-Dose 3D CT Image Reconstruction,” in *The 14th International Meeting on Fully Three-Dimensional Image Reconstruction in Radiology and Nuclear Medicine*, 2017.
- [13] O. Féron, B. Duchêne, and A. Mohammad-Djafari, “Microwave imaging of inhomogeneous objects made of a finite number of dielectric and conductive materials from experimental data,” *Inverse Problems*, vol. 21, no. 6, p. S95, 2005.
- [14] A. Mohammad-Djafari, “Gauss-Markov-Potts Priors for Images in Computer Tomography resulting to Joint Optimal Reconstruction and Segmentation,” *International J. of Tomography and Statistics (IJTS)*, vol. 11, pp. 76–92, 2008.
- [15] H. Ayasso and A. Mohammad-Djafari, “Joint NDT image restoration and segmentation using Gauss–Markov–Potts prior models and variational bayesian computation,” *IEEE Transactions on Image Processing*, vol. 19, no. 9, pp. 2265–2277, 2010.
- [16] N. Zhao, A. Basarab, D. Kouame, and J.-Y. Tournier, “Joint segmentation and deconvolution of ultrasound images using a hierarchical Bayesian model based on generalized Gaussian priors,” *IEEE transactions on Image Processing*, vol. 25, no. 8, pp. 3736–3750, 2016.
- [17] C. Chapdelaine, A. Mohammad-Djafari, N. Gac, and E. Parra, “A 3D Bayesian Computed Tomography Reconstruction Algorithm with Gauss-Markov-Potts Prior Model and its Application to Real Data,” *Fundamenta Informaticae*, vol. 155, no. 4, pp. 373–405, 2017.
- [18] D. Kim, D. Pal, J.-B. Thibault, and J. A. Fessler, “Accelerating ordered subsets image reconstruction for X-ray CT using spatially nonuniform optimization transfer,” *IEEE transactions on medical imaging*, vol. 32, no. 11, pp. 1965–1978, 2013.

- [19] D. Kim, S. Ramani, and J. A. Fessler, "Combining ordered subsets and momentum for accelerated X-ray CT image reconstruction," *IEEE transactions on medical imaging*, vol. 34, no. 1, pp. 167–178, 2015.
- [20] M. G. McGaffin and J. A. Fessler, "Alternating dual updates algorithm for X-ray CT reconstruction on the GPU," *IEEE transactions on computational imaging*, vol. 1, no. 3, pp. 186–199, 2015.
- [21] J. A. Fessler, "Mean and Variance of Implicitly Defined Biased Estimators (such as Penalized Maximum Likelihood): Applications to Tomography," *IEEE Transactions on Image Processing*, vol. 5, no. 3, pp. 493–506, 1996.
- [22] M. Pereyra, "Maximum-A-Posteriori estimation with Bayesian Confidence Regions," *SIAM Journal on Imaging Sciences*, vol. 10, no. 1, pp. 285–302, 2017.
- [23] V. Šmídl and A. Quinn, *The variational Bayes method in signal processing*. Springer Science & Business Media, 2006.
- [24] M. Pereyra, P. Schniter, E. Chouzenoux, J.-C. Pesquet, J.-Y. Tournieret, A. O. Hero, and S. McLaughlin, "A survey of stochastic simulation and optimization methods in signal processing," *IEEE Journal of Selected Topics in Signal Processing*, vol. 10, no. 2, pp. 224–241, 2016.
- [25] N. Bali and A. Mohammad-Djafari, "Bayesian approach with hidden markov modeling and mean field approximation for hyperspectral data analysis," *IEEE Transactions on Image Processing*, vol. 17, no. 2, pp. 217–225, 2008.
- [26] H. Ayasso, B. Duchêne, and A. Mohammad-Djafari, "Bayesian inversion for optical diffraction tomography," *Journal of Modern Optics*, vol. 57, no. 9, pp. 765–776, 2010.
- [27] J.-F. Giovannelli and C. Vacar, "Deconvolution-Segmentation for Textured Images," in *25th European Signal Processing Conference (EUSIPCO)*, pp. 201–205, 2017.
- [28] K. Sauer and C. Bouman, "A local update strategy for iterative reconstruction from projections," *IEEE Transactions on Signal Processing*, vol. 41, no. 2, pp. 534–548, 1993.
- [29] H. Ayasso, *Une approche bayésienne de l'inversion. Application à l'imagerie de diffraction dans les domaines micro-onde et optique*. PhD thesis, Université Paris Sud-Paris XI, 2010.
- [30] J. Besag, "Spatial interaction and the statistical analysis of lattice systems," *Journal of the Royal Statistical Society. Series B (Methodological)*, pp. 192–236, 1974.
- [31] L. Onsager, "Crystal statistics. I. a two-dimensional model with an order-disorder transition," *Physical Review*, vol. 65, no. 3-4, p. 117, 1944.
- [32] K. Huang, *Statistical mechanics*. Wiley, 1987.
- [33] J.-F. Giovannelli, "Estimation of the Ising field parameter thanks to the exact partition function," in *ICIP*, pp. 1441–1444, 2010.
- [34] M. Pereyra, N. Dobigeon, H. Batatia, and J.-Y. Tournieret, "Estimating the granularity coefficient of a Potts-Markov random field within a Markov chain Monte Carlo algorithm," *Image Processing, IEEE Transactions on*, vol. 22, no. 6, pp. 2385–2397, 2013.
- [35] R. Morris, X. Descombes, and J. Zerubia, "Fully Bayesian image segmentation - An engineering perspective," in *Image Processing, 1997. Proceedings., International Conference on*, vol. 3, pp. 54–57, IEEE, 1997.
- [36] R. J. Giordano, T. Broderick, and M. I. Jordan, "Linear response methods for accurate covariance estimates from mean field variational bayes," in *Advances in Neural Information Processing Systems*, pp. 1441–1449, 2015.
- [37] H. Jeffreys, "An invariant form for the prior probability in estimation problems," in *Proceedings of the Royal Society of London a: mathematical, physical and engineering sciences*, vol. 186, pp. 453–461, The Royal Society, 1946.
- [38] J. MacQueen, "Some methods for classification and analysis of multivariate observations," in *Proceedings of the fifth Berkeley symposium on mathematical statistics and probability*, vol. 1, pp. 281–297, Oakland, CA, USA., 1967.
- [39] N. Otsu, "Thresholds selection method form grey-level histograms," *IEEE Trans. On Systems, Man and Cybernetics*, vol. 9, no. 1, p. 1979, 1979.
- [40] F. Kurugollu, B. Sankur, and A. E. Harmanci, "Color image segmentation using histogram multithresholding and fusion," *Image and vision computing*, vol. 19, no. 13, pp. 915–928, 2001.